Scientific Research Publishing

Computational Chemistry, 2024, 12, 75-90
https://www.scirp.org/journal/cc
ISSN Online: 2332-5984
ISSN Print: 2332-5968

DNA Base Pairs Sensors: DFT, QTAIM and NCI-RDG Study

Nour Elyakine Amraoui[1,2*], Dalila Hammoutène[2]

[1]Laboratoire de Chimie des Matériaux et des Vivants: Activité & Réactivité (LCMVAR), Département de Chimie, Faculté des Sciences de la Matière, Université de Batna 1, Batna, Algérie
[2]Laboratoire de Thermodynamique et de Modélisation Moléculaire (LTMM) Faculté de Chimie, USTHB BP 32 Elalia 16111 Bab Ezzouar, Alger, Algérie
Email: *amraoui.nour@yahoo.com

How to cite this paper: Amraoui, N.E. and Hammoutène, D. (2024) DNA Base Pairs Sensors: DFT, QTAIM and NCI-RDG Study. *Computational Chemistry*, **12**, 75-90.
https://doi.org/10.4236/cc.2024.124004

Received: August 28, 2024
Accepted: October 28, 2024
Published: October 31, 2024

Abstract

This work aims to present a theoretical study of sensor candidate formed from Cytosine-Cu-Cytosine at ***DFT/BP86/ZORA/DZP*** level using ADF code for the significance of proposing complexes based on DNA that captures toxic adducts in the gas phase as: **CO**, **CO_2**, **NO**, **HCN**, **SO_2**, **H_2S** and **NO_2**. The interaction between adducts and Cytosine-Cu-Cytosine complex was analyzed by **QTAIM** based on electronic density $\rho(r)$ and Laplacian of electronic density $\nabla^2\rho(r)$. **NCI-RDG** analysis was performed and discussed. Interaction of adducts with Cytosine-Cu-Cytosine complex takes place with a transition state, and the energy barrier is lower with CO_2 E(TS) = 0.26 (kcal/mol). Potential energy surface (PES) gives saddle point for the formation of two bonds Cu-N and Cu-C at $E = -6.826$ a.u, Cu-N = 1.96 Å and Cu-C = 2.38 Å during the interaction of HCN with Cytosine-Cu-Cytosine complex. PES analysis proved that the interaction of NO_2 with Cytosine-Cu-Cytosine achieves stabilization at $E = -6.781$ a.u, $Cu\text{-}N_{NO_2}$ = 2.057 Å and O_{NO_2} …H23 = 1.90 Å.

Keywords

Density Functional Theory (DFT), Sensors, Quantum Theory of Atoms in Molecules (QTAIM), Non-Covalent Interaction Reduced Density Gradient (NCI-RDG), Potential Energy Surface (PES)

1. Introduction

In addition to the biological role of DNA, which is represented by vital in life science [1] [2], transportation of genetic information from one generation to another, DNA bases (adenine, guanine, cytosine and thymine) may be used as attractive

candidates and sensors to detecting some toxic chemical species and proposed as part of safety systems [3]. Moreover, copper is multifunctional, considering that it gets involved in combination with certain proteins to produce enzymes. Copper complexes are used as anticancer drugs, copper ion complexes are used to treat skin problems, and they are also used as sensors and biosensors [4]. Furthermore, copper has a strong affinity to pyrimidine and pyridine structures to form biosensors [5] [6]. Biosensors can be used in a variety of ways. They may provide qualitative information, semi-quantitative information, or provide accurate numbers that can be used to make decisions based on trend information [7]. Metal-mediated base pairs may be used as sensors [8]. Experimentally, the cytosine dimer prefers to combine with the copper ion Cu^{+} at the nitrogen atoms to form stable trans complexes [9]. Toxic species such as: CO_2, CO, SO_2, CH_4 and NH_3 are studied theoretically to be a target for gas sensors [3]. Amino acid-based ionic liquids have a large capacity for carbon dioxide (CO_2) solubility [10]. Meanwhile, polyoxometalate compounds have absorbent efficiency in CO, CO_2, H_2S, NH_3, NO, NO_2, and SO_2 [11]. Therefore, the detection of various gas molecules in the atmosphere is important for academia and industry, and that's why many theoretical and experimental studies have been carried out to reveal the capture of these molecules [12]-[15].

Theoretical chemistry has become a tool for innovation and the proposal of new molecular structures with several applications. we theoretically inspire the role of Cyt-Cu-Cyt complex as a sensor of toxic molecules (CO, CO_2, H_2S, HCN, NO, NO_2, and SO_2). To predict how these adducts interact to Cytosine-Cu-Cytosine complex to form new complexes, it is important to characterize the intermolecular arrangement between them. Intermolecular forces and non-covalent interactions have a significant impact on the structure of biological and non-biological chemistry [16] [17]. For this reason, we have turned to a quantum theory of atoms in molecules (QTAIM), natural bond orbital analysis (NBO), charge transfer, NCI-RDG to predict different forces and interactions between adducts and Cyt-Cu-Cyt complex.

2. Computational Method

All calculations are carried out at **DFT/DZP** level of theory, **GGA-BP86** functional used to predict intermolecular interactions [18] relativistic effect have been taken by **ZORA** the Zero Order Regular Approximated Hamiltonian, energy decomposition analysis. Non-covalent interactions were analyzed and visualized using multiwfn3.7 [19] and VMD programs.

3. Results and Discussion

3.1. Orbital Interaction

The highest occupied molecular orbital (HOMO) and the lowest unoccupied molecular orbital (LUMO) are two important characteristics for analyzing the electronic properties of molecules [20], and the gap between them explains molecular

stability, chemical reactivity and kinetic stability [21]. Generally, HOMO orbital gives electrons while LUMO one accepts them; in our case, LUMO orbital of complex (Cytosine-Cu-Cytosine) has been attacked by HOMO orbital of adducts (NO_2, NO, CO_2, CO, HCN, H_2S, SO_2) (see Figure 1 and Figure 2). Hence, more the energy difference between them is reduced more the attack or the interaction is favored. We observe that the lowest value of the gap (ΔE_{H_2S} = 0.063 eV) was obtained with H_2S molecule, followed by (ΔE_{SO_2} = 0.54 eV) of SO_2 molecule and then by (ΔE_{NO_2} = 0.82 eV) of NO_2 molecule. So, orbital attack of these molecules (NO_2, SO_2 and H_2S) by Cytosine-Cu-Cytosine complex is more favored. Therefore, the orbital interaction will be favored in the following order: ΔE_{H_2S} = 0.063 eV < ΔE_{SO_2} = 0.54 eV < ΔE_{NO_2} = 0.82 eV < ΔE_{NO} = 1.36 eV < ΔE_{HCN} = 2.99 eV < ΔE_{CO_2} = 3.12 eV < ΔE_{CO} = 3.27 Ev.

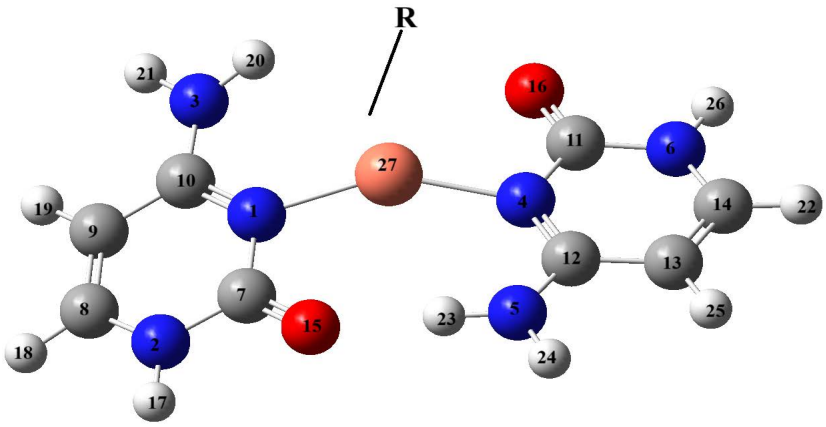

Figure 1. Cytosine-Cu-Cytosine complex with R = NO_2, NO, SO_2, H_2S, CO_2, CO, HCN.

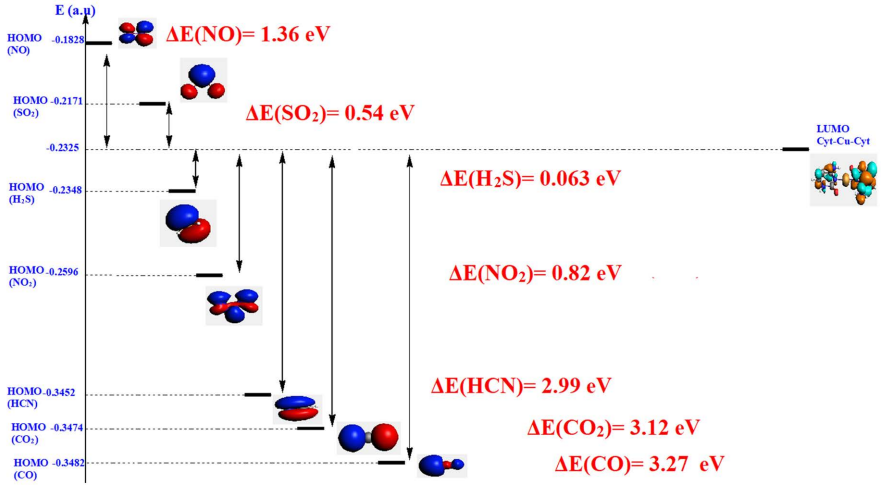

Figure 2. Diagram of HOMO of different molecules (NO, NO_2, H_2S, SO_2, CO_2, CO, HCN) and complex LUMO and their gaps.

3.2. Various Energies

The decomposition of interaction energy is given as [22]:

$$E_{\text{interaction}} = E_{\text{electr}} + E_{\text{orb}} + E_{\text{Pauli}} \quad (1)$$

where E_{elec} is the electrostatic stabilization energy between Cyt-Cu-Cyt and adducts (NO_2, SO_2, CO_2, CO, H_2S, HCN and NO), E_{orb} represents orbital energy at relaxed structures and E_{Pauli} term shows Pauli energy due to repulsion clouds in the molecular geometry. We observe that for all terms, energies are close to each other (Figure 3).

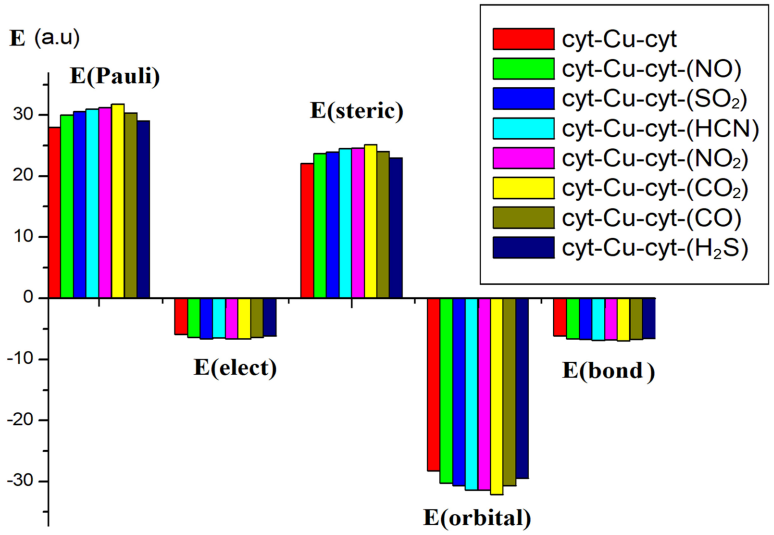

Figure 3. Decomposition energy of various compounds.

E_{Pauli} is destabilizing term for each compound and this destabilizing is offset by E_{orb} and E_{elect}, therefore interaction energy becomes a stabilizing term and varies little from one system to another: ($\boldsymbol{E_{\text{inter}} = -6.07}$ **a.u** for Cyt-Cu-Cyt, $\boldsymbol{E_{\text{inter}} = -6.53}$ **a.u** for Cyt-Cu-Cyt-H_2S, $\boldsymbol{E_{\text{inter}} = -6.58}$ **a.u** for Cyt-Cu-Cyt-NO, $\boldsymbol{E_{\text{inter}} = -6.69}$ **a.u** for Cyt-Cu-Cyt-CO, $\boldsymbol{E_{\text{inter}} = -6.71}$ **a.u** for Cyt-Cu-Cyt-SO_2, $\boldsymbol{E_{\text{inter}} = -6.79}$ **a.u** for Cyt-Cu-Cyt-NO_2, $\boldsymbol{E_{\text{inter}} = -6.84}$ **a.u** for Cyt-Cu-Cyt-HCN and $\boldsymbol{E_{\text{inter}} = -6.95}$ **a.u** for Cyt-Cu-Cyt-CO_2. It is more stabilizing for Cyt-Cu-Cyt-CO_2 complex. On the bonding energy level E_{bond}, this interaction is favored and more stabilizing with CO_2 adduct.

3.3. Transition States

The transition state assumes a special type of chemical equilibrium (quasi-equilibrium) between the initial state (reactants) and the final stable state (products). Our results prove that these interactions occur with transition states since frequency calculations give one imaginary for each case. Figure 4 shows the transition states of the interaction of **CO_2**, **NO**, **CO**, **H_2S** and **SO_2** adducts with Cytosine-Cu-Cytosine complex; these results are performed to form one bond between them (adduct and complex). We noticed that energy barriers vary relatively from one adduct to another and the lowest one is obtained with CO_2 adduct (E_{TS} = 0.26 kcal/mol); hence, we can consider that the interaction with CO_2 is more favored energetically. This energy barrier is followed by (E_{TS} SO_2 = 2.6 kcal/mol), (E_{TS} H_2S = 3.15 kcal/mol), (E_{TS} CO = 6.02 kcal/mol) and (E_{TS} NO = 8.16 kcal/mol).

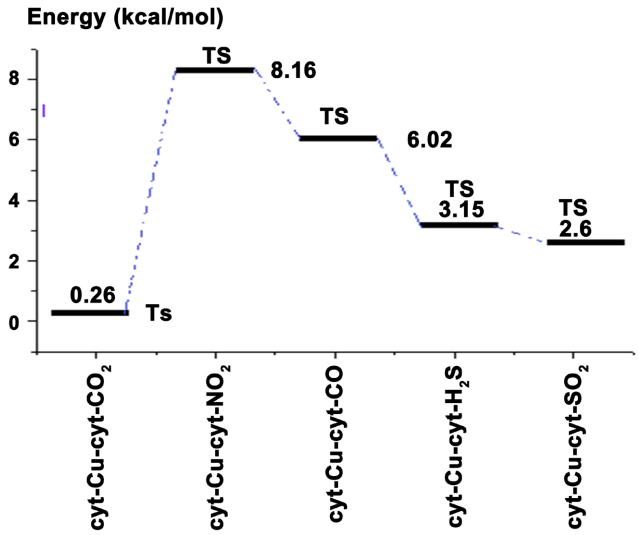

Figure 4. transition states and energy barriers of various interactions.

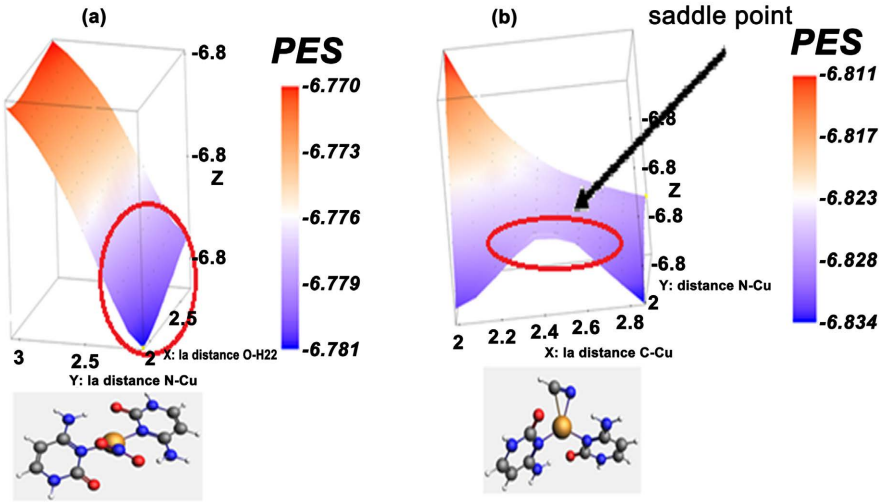

Figure 5. Potential energy surfaces of Cyt-Cu-Cyt-NO_2 (a) and Cyt-Cu-Cyt-HCN (b) complexes.

Interaction of HCN and NO_2 adducts with Cytosine-Cu-Cytosine leads to the formation of two bonds: Cu-N and Cu-C with HCN and Cu-N, O-H23 with NO_2. Potential energy surfaces (PES) are depicted in Figure 5. We notice that a formation of saddle point at (Cu-N = 1.96 Å, Cu-C = 2.38 Å, $E = -6.83$ a.u) during the interaction of HCN with Cytosine-Cu-Cytosine (Figure 5(b)). Regarding the formation of Cytosine-Cu-Cytosine-NO_2, it reaches a minimum at O…H23 = 1.902 Å, Cu-N = 2.057 Å at energy $E = -6.78$ a.u.

3.4. Topological Analysis

Quantum Theory of Atoms in Molecules (QTAIM) Analysis

QTAIM was applied to optimized complexes to quantify and identify intermolecular interactions and the type and structure of bonds [23] [24]. It is based on

electron density analysis [21], more precisely the electron density in "critical point" (cp) is a point in space at which the first derivatives of the density vanish:

$$\nabla\rho = i\frac{\partial\rho}{\partial x} + j\frac{\partial\rho}{\partial y} + k\frac{\partial\rho}{\partial z} \to \begin{cases} \mathbf{0} & (\text{at critical points} \wedge \text{at} \infty) \\ \text{generally} \neq \mathbf{0} & (\text{at all other points}) \end{cases} \quad (2)$$

The second derivatives of $\rho(r)$ can be arranged in the so-called "Hessian matrix", which, when evaluated at a CP located at r_c is written:

$$A(r_c) = \begin{pmatrix} \frac{\partial^2\rho}{\partial x^2} & \frac{\partial^2\rho}{\partial x\partial y} & \frac{\partial^2\rho}{\partial x\partial z} \\ \frac{\partial^2\rho}{\partial y\partial x} & \frac{\partial^2\rho}{\partial y^2} & \frac{\partial^2\rho}{\partial y\partial z} \\ \frac{\partial^2\rho}{\partial z\partial x} & \frac{\partial^2\rho}{\partial z\partial y} & \frac{\partial^2\rho}{\partial z^2} \end{pmatrix}_{r=r_c}$$

The Hessian matrix can be diagonalized and transformed to Λ because it is real and symmetric:

$$\Lambda = \begin{pmatrix} \frac{\partial^2}{\partial x'^2} & 0 & 0 \\ 0 & \frac{\partial^2}{\partial y'^2} & 0 \\ 0 & 0 & \frac{\partial^2}{\partial z'^2} \end{pmatrix}_{r'=r_c} = \begin{pmatrix} \lambda_1 & 0 & 0 \\ 0 & \lambda_2 & 0 \\ 0 & 0 & \lambda_3 \end{pmatrix}$$

In which λ_1, λ_2 and λ_3 are the curvatures of the density. The trace of Hessian matrix of the density is invariant to rotations of the coordinate system and it is known as the Laplacian of the density [$\nabla^2\rho(r)$]:

$$\nabla^2\rho(r) = \nabla\cdot\nabla\rho(r) = \frac{\partial^2\rho(r)}{\partial x^2} + \frac{\partial^2\rho(r)}{\partial y^2} + \frac{\partial^2\rho(r)}{\partial z^2} = \lambda_1 + \lambda_2 + \lambda_3 \quad (3)$$

Figure 6 shows critical points (CP) in Cyt-Cu-Cyt complexes. Those in red represent BCP (bond critical points) while those in green are (RCP) ring critical points. Generally, $\rho(r_c) < 0.07$, $\nabla^2\rho(r_c) > 0$ we have ionic bond, $\rho(r_c) > 0.15$, $\nabla^2\rho(r_c) < 0$ it's about covalent bond and $0.07 < \rho(r_c) < 0.15$, $\nabla^2\rho(r_c) < 0$ it's about an intermediate bond. In the interaction regions, BCP1 was formed during the interaction between the adducts and the Cyt-Cu-Cyt complex, which had low density and positive Laplacian. For that formed between the oxygen atom of CO_2 and N1 of complex BCP1(O-N1) $\left(\rho(r_c), \nabla^2\rho(r_c)\right) = (0.056, 0.173)$ and between the sulfur atom of SO_2 and copper atom BCP1(S-Cu) $\left(\rho(r_c), \nabla^2\rho(r_c)\right) = (0.038, 0.062)$ these criteria are assigned for intermediate closed-shell interaction [21]. About the interaction of CO adduct with Cyt-Cu-Cyt complex BCP1 has $\rho(r)$ = 0.192 a.u with negative Laplacian $\nabla^2\rho(r) = -0.159$ a.u and hence BCP1(C_{CO}-Cu) is assigned as a covalent bond. Low density and positive Laplacian are assigned for the interaction of NO and H_2S adducts with Cyt-Cu-Cyt complex; BCP1(N_{NO}-Cu) have $\left(\rho(r_c), \nabla^2\rho(r_c)\right) = (0.106 \text{ a.u}, 0.096 \text{ a.u})$, BCP1(S_{H_2S}-Cu) have $\left(\rho(r_c), \nabla^2\rho(r_c)\right) = (0.077 \text{ a.u}, 0.109 \text{ a.u})$, these parameters correspond to

electrostatic interactions. For N-Cu bonds, electronic density ranges from [0.065 a.u] to [0.173 a.u] and Laplacian varies in the interval [0.05 a.u, 0.271 a.u]. We can scribe them as electrostatic interaction. Exception for N4-Cu bond in Cyt-Cu-Cyt-CO_2 complex which has negative Laplacian $\nabla^2\rho(r_c) = -0.11$ a.u , so it is considered as a covalent bond. In the interaction region, it was formed pseudo cycle characterized by a ring critical point having low electronic density from $\rho(r_c) = 0.007$ a.u to $\rho(r_c) = 0.01$ a.u . QTAIM performs hydrogen bonds with very low values of electronic density from $\rho(r_c) = 0.028$ a.u to $\rho(r_c) = 0.034$ a.u with positive Laplacian.

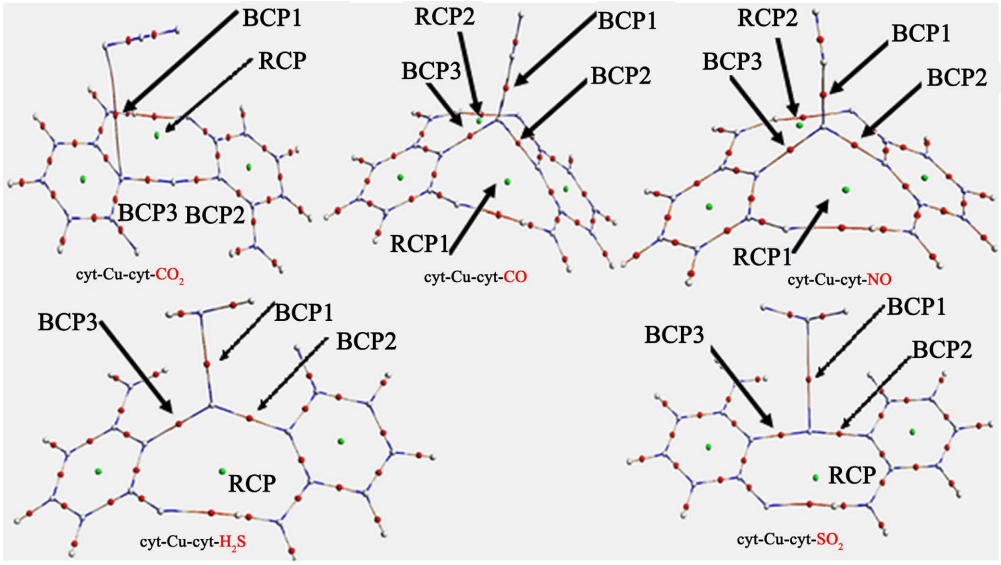

Figure 6. Bond critical points (BCPs) (red), ring critical points (RCPs) (green) of Cyt-Cu-Cyt complex with different adducts (CO_2, CO, NO, H_2S and SO_2).

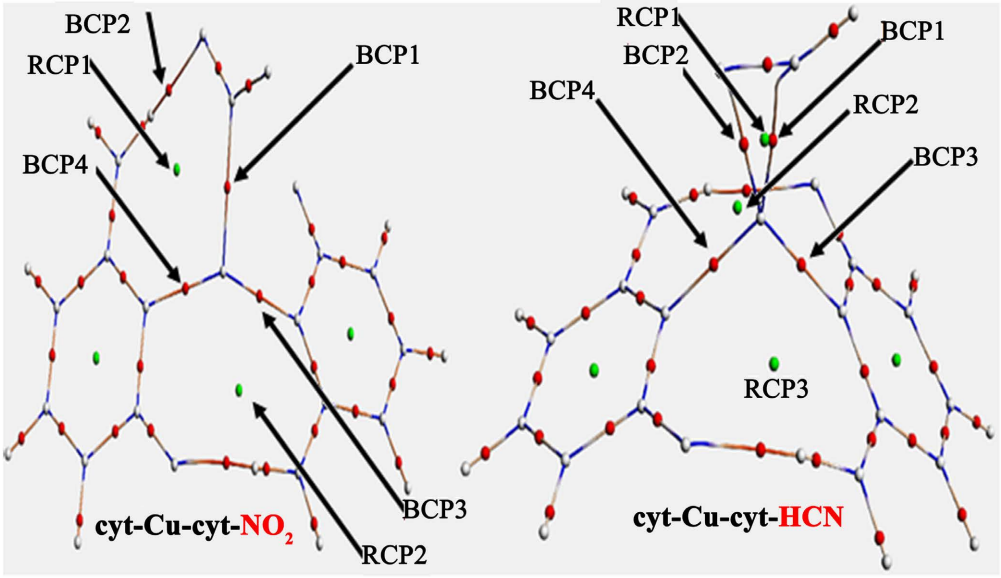

Figure 7. Bond critical points (BCPs) (red), ring critical points (RCPs) (green) of Cyt-Cu-Cyt complex with different adducts (NO_2 and HCN).

Figure 7 exposes topological properties of Cyt-Cu-Cyt-NO_2 and Cyt-Cu-Cyt-HCN complexes. One bond was formed during the interaction of NO_2 with Cyt-Cu-Cyt complex, more precisely between N_{NO_2} and Cu whose critical point atoms BCP1 having $\left(\rho(r_c),\nabla^2\rho(r_c)\right)=(0.065\text{ a.u},0.117\text{ a.u})$ According to these criteria (low electronic density and positive Laplacian), we can assign it as electrostatic interaction. The interaction of HCN adduct with Cyt-Cu-Cyt complex leads to the form of two bonds: C_{HCN}-Cu having BCP1 characterized by $\left(\rho(r_c),\nabla^2\rho(r_c)\right)=(0.102\text{ a.u},0.248\text{ a.u})$, the second one BCP2, was formed between N_{HCN}-Cu having ($\left(\rho(r_c),\nabla^2\rho(r_c)\right)=(0.106\text{ a.u},0.286\text{ a.u})$ it is also assigned as electrostatic interaction. In this way, it formed a ring with three atoms (Cu-C-N) characterized by RCP1 $\nabla^2\rho(r_c)=0.092$ a.u . Likewise, Cu-N bonds have low values of electronic density ranging from [0.071 a.u] to [0.143 a.u] and positive Laplacian in the range [0.023 a.u - 0.199 a.u], so we can assign them as intermediate closed-shell interaction. Ring critical points have a very low electronic density from [0.008 a.u] to [0.092 a.u]. It was formed a new hydrogen bond between O_{NO_2} ….H20 having BCP2 with ($\left(\rho(r_c),\nabla^2\rho(r_c)\right)=(0.033\text{ a.u},0.119\text{ a.u})$. The other hydrogen bonds also have a low electronic density from [0.031 a.u] to [0.111 a.u] and positive Laplacian in the range [0.031 a.u] to [0.391 a.u] and hence they are assigned as intermediate closed-shell interaction.

3.5. Covalent and Non-Covalent Part of Bonds

Table 1 displays covalent and non-covalent percentage of various bonds as well as their bond energies. From results, it can be observed that Cu-C_{CO}, Cu-O_{CO_2} and Cu-C_{HCN} bonds possess a high non-covalent character which is equal to 97.8% (74.8 kcal/mol) and 89.1% (72.73 kcal/mol) 98.6% (9.5 kcal/mol) respectively, and it is more stabilizing with CO. We also notice that Cu-N_{NO}, Cu-N_{NO_2}, Cu-O_{NO_2}, Cu-N_{NO_2} and Cu-N_{HCN} bonds hybrid character between covalent and non-covalent interactions having the following values: for covalent part 58.3% (539.28 kcal/mol), 98.1% (36.99), 94%, 97.4% and 43.5% (86.21 kcal/mol) respectively and it is more stabilizing with Cu-N_{NO}. For non-covalent parts, 41.7% (748.06 kcal/mol), 1.9% (5.89 kcal/mol), 6% (61.74 kcal/mol), 2.6% (65.14 kcal/mol) and 56.5% (111.87 kcal/mol) respectively and it is more stabilizing with Cu-N_{NO}. Hybrid character is also dominant in Cu-N1 and Cu-N4 bonds, giving a mixture of covalent and non-covalent interaction for the majority of complexes, except for Cyt-Cu-Cyt-NO which are purely covalent bonds. Cu-S_{SO_2} bond is purely non-covalent, having (130.82 kcal/mol) whereas Cu-S_{H_2S} bond is mostly covalent 95.7% (83.10 kcal/mol). Hydrogen bonds are described as non-covalent interactions with very low covalent character.

Table 1. Covalent part, non-covalent (%) part and bond energy (kcal/mol) of different bonds.

Bond	Bond length (Å)	Covalent part %	Non-covalent part%
Cyt-Cu-cyt-CO			
Cu-Cco	1.80	2.2 (1.61)	97.8 (74.8)

Continued

Cu-N1	1.99	2.3 (6.2)	97.7 (−68.99)
Cu-N4	2.004	36.7 (73.58)	63.3 (126.66)
Cu-O15	2.78	8.1 (−7.65)	91.9 (−87.25)
Cu-O16	2.89	11.2 (−10.8)	88.8 (−85.95)
O15…H23	1.98	0.3 (−0.10)	99.7 (−38.49)
O16…H20	1.91	1.9 (−1.15)	98.1 (−60.92)
Cyt-Cu-cyt-CO_2			
Cu-N4	1.87	51.7 (−102.7)	48.3 (−110.06)
Cu-N1	1.86	47.7 (−103.39)	52.3 (−113.24)
Cu-O(CO_2)	3.66	10.9 (8.89)	89.1 (72.73)
N1-O(CO)	3.29	17.5 (−19.95)	82.5 (134.04)
O15…H23	2.134	0.2 (−0.01)	99.8 (−8.25)
O16…H20	3.31	1.3 (−0.13)	98.7 (−9.81)
Cyt-Cu-cyt-SO_2			
Cu-S	2.74	0 (0)	100 (130.82)
Cu-N1	1.87	46.3 (−99.81)	53.7 (−115.58)
Cu-N4	1.88	4.6 (−3.16)	95.4 (−65.14)
O15…H23	3.51	1.7 (−1.7)	99.3 (−60.61)
O16…H20	2.015	1.5 (−0.14)	98.5 (−9.04)
Cu-O17	3.45	5.4 (−3.67)	94.6 (−63.93)
Cu-O18	3.39	5.9 (−4.09)	94.1 (64.90)
Cyt-Cu-cyt-NO			
Cu-N(NO)	1.82	58.3 (539.28)	41.7 (748.06)
Cu-N1	1.99	100 (88.57)	0
Cu-N4	2.00	100 (75.41)	0
O15…H23	1.94	0.1 (−0.04)	99.9 (−25.88)
O16…H20	1.93	1.3 (−0.09)	98.7 (−6.68)
Cyt-Cu-cyt-NO_2			
Cu-N(NO_2)	2.06	98.1 (36.99)	1.9 (5.89)
Cu-N1	1.95	77.6 (36.64)	22.4 (−30.75)
Cu-N4	1.96	90.8	9.2 (12.14)
O15…H23	3.94	0	100 (0.09)
O16…H20	1.92	1.5 (0.10)	98.5 (6.26)
O(NO_2)…H23	1.90	49.3 (31.09)	50.7 (32.09)
Cu-O(NO_2)	2.83	94	6 (61.74)
Cu-O(NO_2)	2.83	97.4	2.6 (65.14)
Cyt-Cu-cyt-HCN			
Cu-N1	1.95	39.4 (82.34)	60.6 (126.73)

Continued

Cu-N4	2.00	36 (71.60)	94 (127.23)
Cu-N (HCN)	1.96	43.5 (86.21)	56.5 (111.87)
Cu-C(HCN)	1.99	2.4 (0.13)	98.6 (9.5)
O15…H23	1.97	1.4 (0.13)	98.6 (9.15)
O16…H20	1.87	1.8 (1.1)	98.2 (60.45)
Cyt-Cu-cyt-H_2S			
Cu-S	2.30	95.7 (83.10)	4.3 (3.45)
Cu-N1	1.99	44.9 (81.28)	55.1 (99.67)
Cu-N4	1.99	43.8 (80.12)	56.2 (102.76)
Cu-O(SO_2)	2.95	9 (6.9)	91 (69.91)
Cu-O(SO_2)	2.86	11.2 (0.84)	88.8 (6.67)
O15…H23	1.83	16.5 (15.06)	83.5 (76.00)
O16…H20	3.52	0.3 (0.11)	99.7 (39.56)

Values between parenthesis are bond energies in (kcal/mol).

3.6. Non-Covalent Interaction Reduced Density Gradient Analysis (NCI-RDG)

Reduced density gradient (RDG) approach used to reveal non-covalent intermolecular and intramolecular interactions [25]. It is a visualization index based on electronic density and its derivatives using RDG results at low densities [26] [27]:

$$\mathrm{RDG}(r)=\frac{1}{2\left(3\pi^2\right)^{\frac{1}{3}}}\frac{\left|\Delta\rho(r)\right|}{\rho(r)^{\frac{4}{3}}} \tag{4}$$

According to the sign $\lambda_2\rho$ (the second eigenvalue of the electronic density Hessian matrix), we can identify the nature of interaction: sign $\lambda_2\rho < 0$ signifies a strong attractive interaction such as a hydrogen bond, sign $\lambda_2\rho > 0$ denotes a steric interaction. If sign $\lambda_2\rho \approx 0$, that implies weak attractive interaction such as Van der Waals interactions.

Figure 8 and Figure 9 show reduced density gradient (RDG) scatters and non-covalent interaction (NCI) plots respectively of Cyt-Cu-Cyt-CO, Cyt-Cu-Cyt-CO_2, Cyt-Cu-Cyt-NO, Cyt-Cu-Cyt-NO_2, Cyt-Cu-Cyt-SO_2 complexes. The appearance of spikes in scatters indicates the existence of such interaction. We observed for most of these complexes, localization of spikes at sign $\lambda_2(\rho) < 0$ from −0.05 to −0.02 a.u indicating the strong character of hydrogen bonds, which is visualized by blue color in NCI plots of Cyt-Cu-Cyt-CO, Cyt-Cu-Cyt-NO, Cyt-Cu-Cyt-NO_2 and Cyt-Cu-Cyt-SO_2 complexes. Whereas, for Cyt-Cu-Cyt-CO_2 complex, strong non-covalent interaction is represented at sign $\lambda_2(\rho) = -0.02$ a.u. In the near of zero sign $\lambda_2(\rho) \approx 0$, Van der Waals interactions are represented at −0.01 a.u, 0.01 a.u and visualized by green color in various plots. When sign $\lambda_2(\rho) > 0$ exactly (from 0.02 a.u to 0.03 a.u) designating steric effect of the two rings

of Cytosine that visualized by red color in different plots. These results are in good agreement with QTAIM analysis confirming the blending interaction at linking region of various complexes.

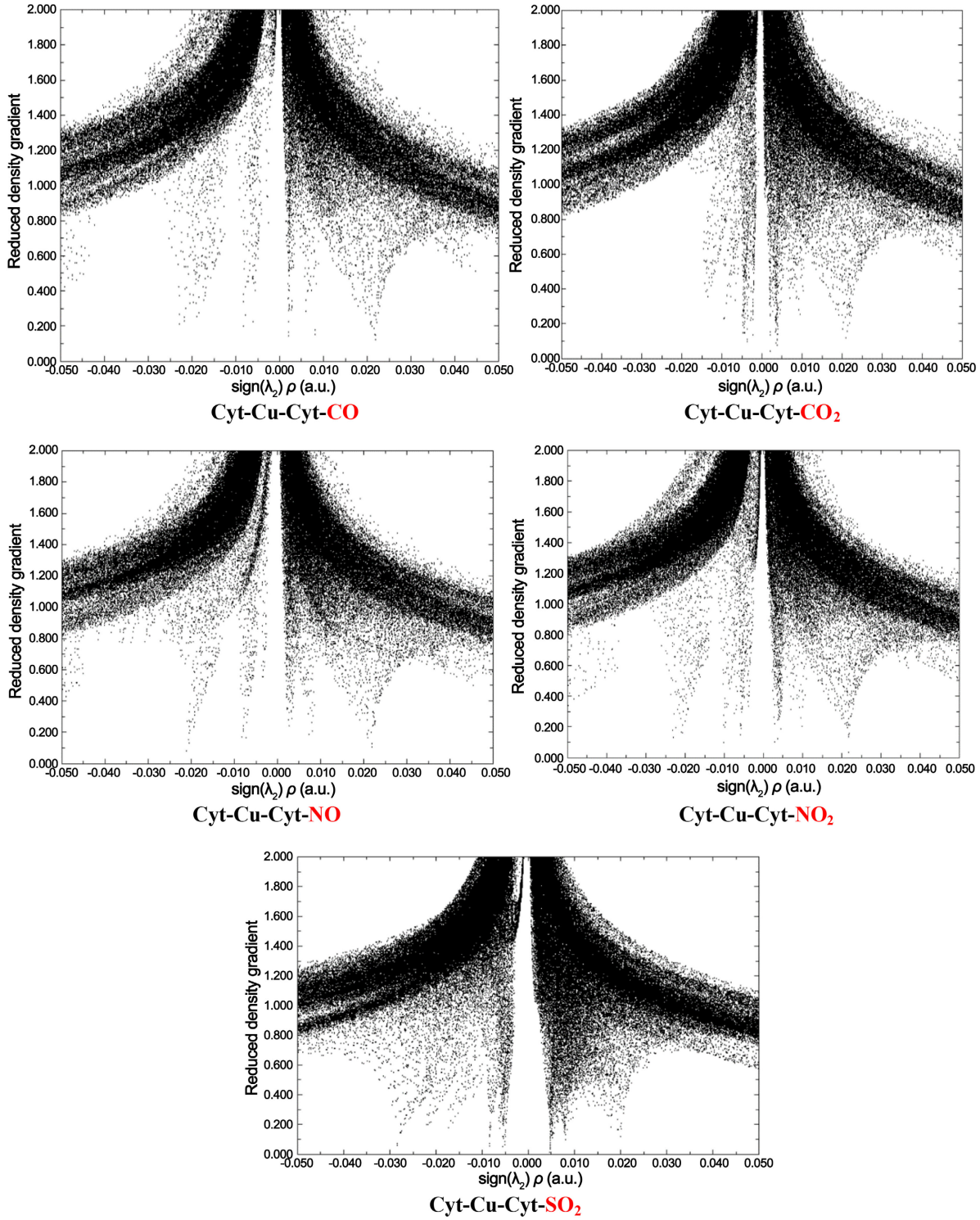

Figure 8. Reduced density gradient (RDG) as a function of sign λ_2 ρ (the second eigenvalue of the electronic density Hessian matrix) of Cyt-Cu-Cyt-CO, Cyt-Cu-Cyt-CO_2, Cyt-Cu-Cyt-NO, Cyt-Cu-Cyt-NO_2, Cyt-Cu-Cyt-SO_2 complexes.

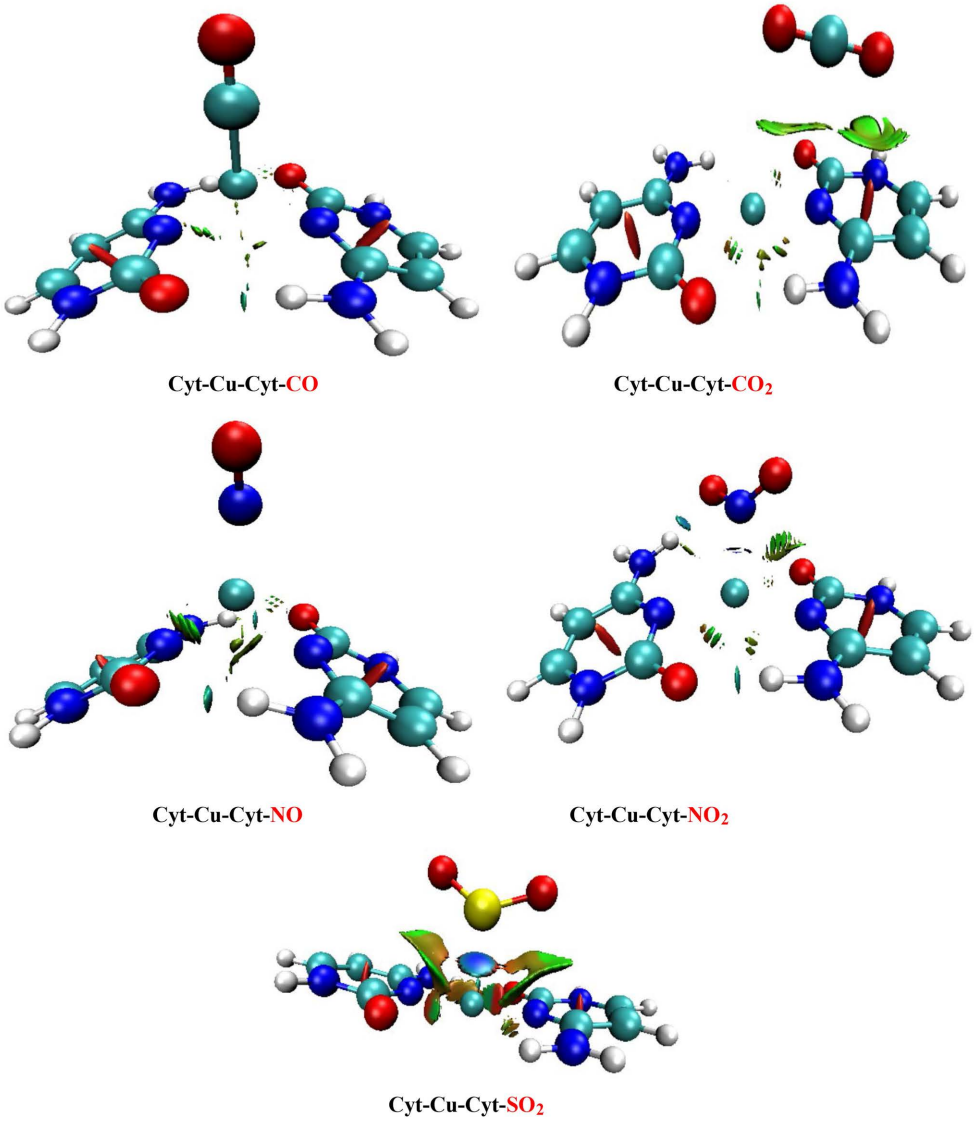

Figure 9. Non-covalent interaction (NCI) plots of Cyt-Cu-Cyt-CO, Cyt-Cu-Cyt-CO_2, Cyt-Cu-Cyt-NO, Cyt-Cu-Cyt-NO_2, Cyt-Cu-Cyt-SO_2 complexes.

Figure 10 and Figure 11 show reduced density gradient (RDG) and Non-covalent interaction (NCI) plots respectively of Cyt-Cu-Cyt-HCN, Cyt-Cu-Cyt-H_2S complexes. Likewise, sign $\lambda_2 < 0$ indicates strong interaction or hydrogen bond, more precisely from (−0.05 a.u to −0.02 a.u) for Cyt-Cu-Cyt-HCN and which is represented by blue color between NH…O atoms of thymine bases. Hydrogen bond is absent in Cyt-Cu-cyt-H_2S complex, but there exists a strong interaction between sulfur atom and copper ion. Weak interactions are designated at sign $\lambda_2 \approx 0$ it belongs to the interval [−0.01 a.u, −0.01 a.u] for the two complexes denoting Van der Waals interactions that are visualized by green color and that are very marked in Cyt-Cu-Cyt-HCN complex. While, positive sign λ_2 $\rho(r)$ in the range [0.02 a.u, 0.05 a.u] specifies steric effects that are visualized by red color for the two complexes.

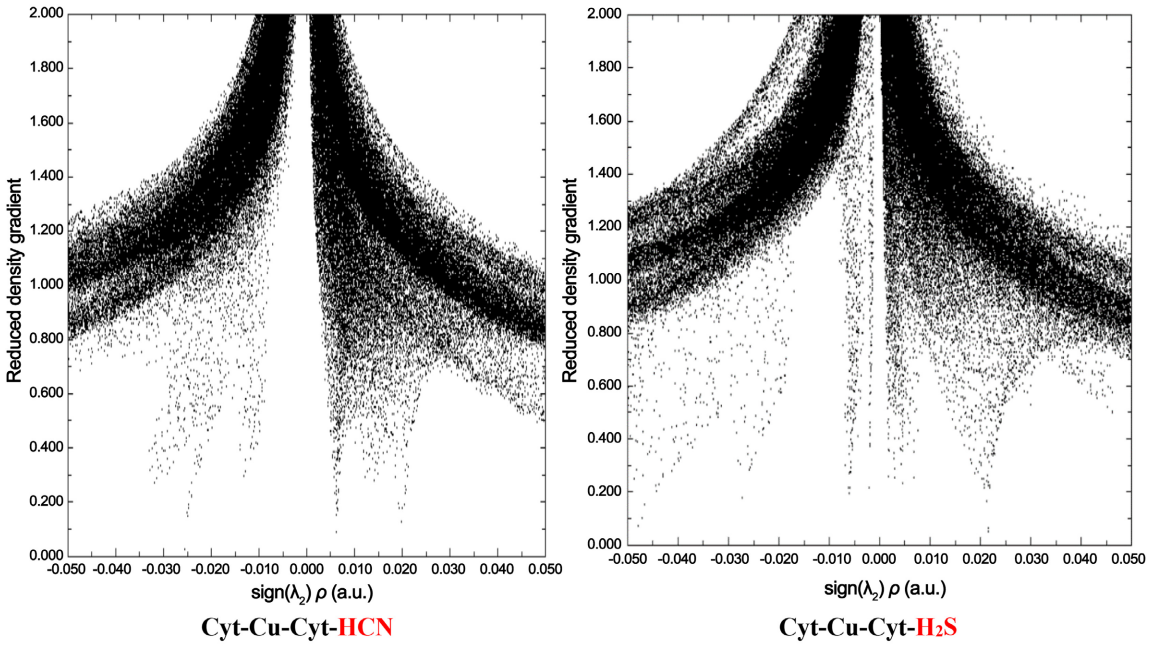

Figure 10. Reduced density gradient (RDG) as a function of sign $\lambda_2\,\rho$ (the second eigenvalue of the electronic density Hessian matrix) of Cyt-Cu-Cyt-HCN, Cyt-Cu-Cyt-H_2S.

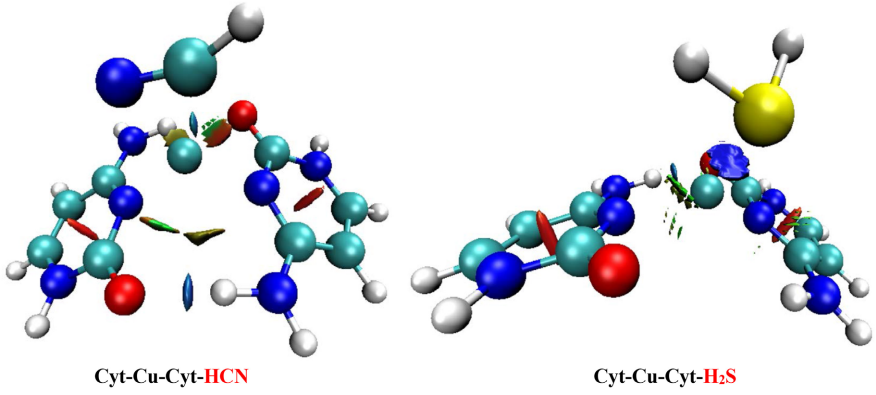

Figure 11. Non-covalent interaction (NCI) plots of Cyt-Cu-Cyt-HCN, Cyt-Cu-Cyt-H_2S complexes.

4. Conclusion

In this work, we carried out a theoretical study at DFT/BP86/DZP/ZORA level of the interaction of Cyt-Cu-Cyt complex as a sensor with certain adducts (CO, CO_2, NO, NO_2, HCN, H_2S and SO_2). Our results prove that the lowest value of the gap (ΔE_{H_2S} = 0.063 eV) obtained with H_2S molecule and hence H_2S interaction with Cyt-Cu-Cyt is more favored. Decomposition energies: electrostatic energy, Pauli energy and orbital energy are offset between them to achieve stabilization of each electronic system. Our results attest that the interaction of **CO_2, NO, CO, H_2S** and **SO_2** transition state and interaction with CO_2 is more favored energetically. Potential energy surfaces (PES) proves the formation of saddle point at (Cu-N = 1.96 Å, Cu-C = 2.38 Å, E = −6.83 a.u) during the interaction of HCN with Cytosine-

Cu-Cytosine, while it reaches a minimum at O…H23 = 1.902 Å, Cu-N = 2.057 Å and at energy $E = -6.78$ a.u for the interaction of NO_2 with Cyt-Cu-Cyt. QTAIM and NCI-RDG analysis prove that most bonds have a mixture of character, covalent and non-covalent.

Conflicts of Interest

The authors declare no conflicts of interest regarding the publication of this paper.

References

[1] Minchin, S. and Lodge, J. (2016) Understanding Biochemistry: Structure and Function of Nucleic Acids. *Essays in Biochemistry Journal*, **63**, 1010-1017.

[2] Thompson, J.J., Kaur, R., Sosa, C.P., Lee, J., Kashiwagi, K., Zhou, D., *et al.* (2018) ZBTB24 Is a Transcriptional Regulator That Coordinates with DNMT3B to Control DNA Methylation. *Nucleic Acids Research*, **46**, 10034-10051. https://doi.org/10.1093/nar/gky682

[3] Rad, A.S., Nasimi, N., Jafari, M., Shabestari, D.S. and Gerami, E. (2015) *Ab-Initio* Study of Interaction of Some Atmospheric Gases (SO_2, NH_3, H_2O, CO, CH_4 and CO_2) with Polypyrrole (3PPy) Gas Sensor: DFT Calculations. *Sensors and Actuators B: Chemical*, **220**, 641-651. https://doi.org/10.1016/j.snb.2015.06.019

[4] Chopra, T., Sasan, S., Devi, L., Parkesh, R. and Kapoor, K.K. (2022) A Comprehensive Review on Recent Advances in Copper Sensors. *Coordination Chemistry Reviews*, **470**, Article ID: 214704. https://doi.org/10.1016/j.ccr.2022.214704

[5] Vural, H. (2022) A Novel Copper (II) Complex Containing Pyrimidine-4-Carboxylic Acid: Synthesis, Crystal Structure, DFT Studies, and Molecular Docking. *Journal of Molecular Structure*, **1265**, Article ID: 133390. https://doi.org/10.1016/j.molstruc.2022.133390

[6] Liu, Y., Zhang, Q., Yao, S., Cui, H., Zou, Y. and Zhao, L. (2024) Dual-Recognition "Turn-off-On" Fluorescent Biosensor Triphenylamine-Based Continuous Detection of Copper Ion and Glyphosate Applicated in Environment and Living System. *Journal of Hazardous Materials*, **477**, Article ID: 135216. https://doi.org/10.1016/j.jhazmat.2024.135216

[7] Tukadiya, N.A., Jana, S.K., Chakraborty, B. and Jha, P.K. (2023) C_{24} Fullerene and Its Derivatives as a Viable Glucose Sensor: DFT and TD-DFT Studies. *Surfaces and Interfaces*, **41**, Article ID: 103220. https://doi.org/10.1016/j.surfin.2023.103220

[8] Hebenbrock, M. and Müller, J. (2023) Metal-Mediated Base Pairs in Nucleic Acid Duplexes. In: Reedijk, J. and Poeppelmeier, K.R., Eds., *Comprehensive Inorganic Chemistry III*, 3rd Edition, Elsevier, 664-713. https://doi.org/10.1016/b978-0-12-823144-9.00033-9

[9] Gao, J., Berden, G., Rodgers, M.T. and Oomens, J. (2016) Interaction of Cu^+ with Cytosine and Formation of I-Motif-Like C-M^+-C Complexes: Alkali versus Coinage Metals. *Physical Chemistry Chemical Physics*, **18**, 7269-7277. https://doi.org/10.1039/c6cp00234j

[10] Noorani, N. and Mehrdad, A. (2020) CO_2 Solubility in Some Amino Acid-Based Ionic Liquids: Measurement, Correlation and DFT Studies. *Fluid Phase Equilibria*, **517**, Article ID: 112591. https://doi.org/10.1016/j.fluid.2020.112591

[11] Syamlal, S.K., Sarath Kumar, C.B., Reji, R.P., Roshal, P.S., Sivalingam, Y. and Surya, V.J. (2022) Hydration Effect of Selected Atmospheric Gases with Finite Water

Clusters: A Quantum Chemical Investigation Towards Atmospheric Implications. *Chemosphere*, **307**, Article ID: 135947. https://doi.org/10.1016/j.chemosphere.2022.135947

[12] Dziejarski, B., Serafin, J., Andersson, K. and Krzyżyńska, R. (2023) CO_2 Capture Materials: A Review of Current Trends and Future Challenges. *Materials Today Sustainability*, **24**, Article ID: 100483. https://doi.org/10.1016/j.mtsust.2023.100483

[13] Chaabene, M., Gassoumi, B., Soury, R., Ghalla, H., Jabli, M., Ben Chaâbane, R., *et al.* (2021) Insights into Theoretical Detection of CO_2, NO, CO, O_2, and O_3 Gases Molecules Using Zinc Phthalocyanine with Peripheral Mono and Tetra Quinoleinoxy Substituents: Molecular Geometries, Electronic Properties, and Vibrational Analysis. *Chemical Physics*, **547**, Article ID: 111198. https://doi.org/10.1016/j.chemphys.2021.111198

[14] Xiong, H., Zhang, H. and Gan, L. (2021) A New Bifunctional C_3N Nanosheet of NO_2, SO_2 Gas Sensor and CO_2 Separation: A First-Principles Study. *Physica E: Low-Dimensional Systems and Nanostructures*, **126**, Article ID: 114463. https://doi.org/10.1016/j.physe.2020.114463

[15] Demirci, S. and Sahiner, N. (2020) The Use of Conductive Polymers Embedded Macro Porous Pei and Ionic Liquid Form of Pei Cryogels for Potential Conductometric Sensor Application to CO_2. *Journal of Composites Science*, **4**, Article No. 27. https://doi.org/10.3390/jcs4010027

[16] Jumabaev, A., Holikulov, U., Hushvaktov, H., Issaoui, N. and Absanov, A. (2023) Intermolecular Interactions in Ethanol Solution of OABA: Raman, FTIR, DFT, M062X, MEP, NBO, FMO, AIM, NCI, RDG Analysis. *Journal of Molecular Liquids*, **377**, Article ID: 121552. https://doi.org/10.1016/j.molliq.2023.121552

[17] Al-Mutairi, A.A., Katari, B.K.P., Narasimhan, Y., Blacque, O., Al-Wahaibi, L.H., Al-Alshaikh, M.A., *et al.* (2020) Interplay of Weak Intermolecular Interactions in Two Schiff's Bases with Organic Fluorine Derived from 5-Nitrothiophene-2-Carboxaldehyde: Crystal Structures, DFT Calculation and *in Vitro* Evaluation of Bioactivities. *Journal of Molecular Structure*, **1221**, Article ID: 128883. https://doi.org/10.1016/j.molstruc.2020.128883

[18] Orio, M., Pantazis, D.A. and Neese, F. (2009) Density Functional Theory. *Photosynthesis Research*, **102**, 443-453. https://doi.org/10.1007/s11120-009-9404-8

[19] Lu, T. and Chen, F. (2011) Multiwfn: A Multifunctional Wavefunction Analyzer. *Journal of Computational Chemistry*, **33**, 580-592. https://doi.org/10.1002/jcc.22885

[20] Alghamdi, S.K., Abbas, F., Hussein, R.K., Alhamzani, A.G. and El-Shamy, N.T. (2023) Spectroscopic Characterization (IR, Uv-Vis), and HOMO-LUMO, MEP, NLO, NBO Analysis and the Antifungal Activity for 4-Bromo-N-(2-Nitrophenyl) Benzamide; Using DFT Modeling and in Silico Molecular Docking. *Journal of Molecular Structure*, **1271**, Article ID: 134001. https://doi.org/10.1016/j.molstruc.2022.134001

[21] Isravel, A.D., Jeyaraj, J.K., Thangasamy, S. and John, W.J. (2021) DFT, NBO, HOMO-LUMO, NCI, Stability, Fukui Function and Hole—Electron Analyses of Tolcapone. *Computational and Theoretical Chemistry*, **1202**, Article ID: 113296. https://doi.org/10.1016/j.comptc.2021.113296

[22] Amraoui, N.E. and Hammoutène, D. (2015) DFT Study and Topological Analysis of the Bonding in DNA Hoogsteen-Type Base Pairs. *Journal of Theoretical and Computational Chemistry*, **14**, Article ID: 1550047. https://doi.org/10.1142/s0219633615500479

[23] Cukrowski, I., de Lange, J.H., Adeyinka, A.S. and Mangondo, P. (2015) Evaluating Common QTAIM and NCI Interpretations of the Electron Density Concentration

through IQA Interaction Energies and 1D Cross-Sections of the Electron and Deformation Density Distributions. *Computational and Theoretical Chemistry*, **1053**, 60-76. https://doi.org/10.1016/j.comptc.2014.10.005

[24] Shahbazian, S. (2023) The MC-QTAIM: A Framework for Extending the "Atoms in Molecules" Analysis beyond Purely Electronic Systems. In: Rodríguez, J.I., *et al*., Eds., *Advances in Quantum Chemical Topology beyond QTAIM*, Elsevier, 73-109. https://doi.org/10.1016/b978-0-323-90891-7.00017-7

[25] Sukanya, R., Aruldhas, D., Hubert Joe, I. and Balachandran, S. (2022) Spectroscopic and Quantum Chemical Computation on Molecular Structure, AIM, ELF, RDG, NCI, and NLO Activity of 4-VINYL Benzoic Acid: A DFT Approach. *Journal of Molecular Structure*, **1253**, Article ID: 132273. https://doi.org/10.1016/j.molstruc.2021.132273

[26] Tamafo Fouegue, A.D., Nono, J.H., Nkungli, N.K. and Ghogomu, J.N. (2020) A Theoretical Study of the Structural and Electronic Properties of Some Titanocenes Using DFT, TD-DFT, and QTAIM. *Structural Chemistry*, **32**, 353-366. https://doi.org/10.1007/s11224-020-01630-9

[27] Roufieda Guerroudj, A., Ullah Mughal, E., Naeem, N., Sadiq, A., Al-Fahemi, J.H., Asghar, B.H., *et al*. (2024) Exploring Pyrimidine-Based Azo Dyes: Vibrational Spectroscopic Assignments, TD-DFT Investigation, Chemical Reactivity, HOMO-LUMO, ELF, LOL and NCI-RDG Analysis. *Spectrochimica Acta Part A*: *Molecular and Biomolecular Spectroscopy*, **313**, Article ID: 124093. https://doi.org/10.1016/j.saa.2024.124093